Non-enzymatic simultaneous detection of L-glutamic acid and uric acid using mesoporous Co₃O₄ nanosheets†

Mohammad Musarraf Hussain,[ab] Mohammed M. Rahman,[*ab] Abdullah M. Asiri[ab] and Md. Rabiul Awual[c]

Cobalt oxide nanosheets (Co₃O₄ NSs) were synthesized by a facile wet-chemical technique at low-temperature in the alkaline phase. The Co₃O₄ NSs were characterized using various conventional methods, such as Fourier-transform infrared spectroscopy (FTIR), ultraviolet visible spectroscopy (UV/Vis), field emission scanning electron microscopy (FESEM) equipped with X-ray electron dispersive spectroscopy (XEDS), X-ray photoelectron spectroscopy (XPS), Brunauer−Emmett−Teller (BET) studies, powder X-ray diffraction (XRD), *etc*. Simultaneously, two selective L-glutamic acid (L-GA) and uric acid (UA) biological sensors were obtained *via* the fabrication of a thin layer of NSs onto a glassy carbon electrode (GCE, surface area: 0.0316 cm^2). Improved electrochemical performance such as higher sensitivity, linear dynamic range (LDR) and long term stability of the preferred L-GA and UA has been achieved using a reliable I−V method. The calibration curves of L-GA and UA are found to be linear ($R^2 = 0.889$ and 0.901) over a wide range of concentrations (0.1 nM to 0.1 M). Based on a signal-to-noise ratio of 3, the sensor sensitivity and limit of detection (LOD) of L-GA and UA were calculated to be 9.5×10^{-5} and 1.6×10^{-4} μA μM^{-1} cm^{-2}, and 10.0 and 60.0 pM, respectively. The synthesis of Co₃O₄ NSs by a wet chemical route is an outstanding approach for the development of nanomaterial based biosensors to aid enzyme-free detection in healthcare fields. Finally, the proposed Co₃O₄ NSs sensor was applied in the selective detection of L-GA and UA simultaneously in real samples such as serum and urine and found to give acceptable and reasonable results.

1   Introduction

Biosensors are an effective analytical tool with high sensitivity, short turnaround time, specificity and stability and are applied in both research (clinical and diagnosis) and in industry.[1] Electrochemical biosensors are acquiescent, fast, inexpensive and susceptible in the field of life sciences.[2] Extensive efforts have been made over the previous decade to create new biosensors for elementary studies in biotechnology and natural sciences such as the assessment of analyte levels and enzyme activity and the recognition of bimolecular agents (oligonucleotides including proteins and sugars). Different classical techniques such as electrochemical signal transduction, fluorescence, surface-enhanced Raman spectroscopy and surface plasmon resonance have been developed for the detection of biomolecules. Among them, an electrochemical signal transduction procedure holds advantages over other transduction techniques in terms of accuracy, expense, security, selectivity and sensitivity.[3]

Nanotechnology has explored the exceptional properties of low-dimensional heterostructures that enhanced electron–hole pair recombination and size-dependent modification of spectral emission towards short wavelengths.[4,5] The efficiency of nanostructured materials can be higher and a device may be proposed from these criteria to work towards the development of a biosensor at a lower threshold operating voltage.[6] One and zero dimensional nanostructures (nanoneedles including nanorods and nanowires) have attracted keen interest in the area of nanotechnology due to their electrical, electronic, optical and optoelectronic distinctiveness. Inorganic nanoparticles have garnered huge interest in nanotechnology and nanoscience and have an expansive range of applications. NSs present outstanding electronic, magnetic, mechanical, optical and thermal characteristics that arise noticeably from their nanometer area.[7] The latest advancements in the areas of material science and nanotechnology have enabled actual time monitoring of electroactive biomolecules by using different

[a]Chemistry Department, King Abdulaziz University, Faculty of Science, Jeddah 21589, P. O. Box 80203, Saudi Arabia

[b]Center of Excellence for Advanced Material Research (CEAMR), King Abdulaziz University, Jeddah 21589, P. O. Box 80203, Saudi Arabia. E-mail: mmrahman@kau.edu.sa; mmrahmanh@gmail.com; Fax: +966-0126952292; Tel: +966-59-6421830

[c]Actinide Chemistry Group, Material Sciences and Research Centre, Japan Atomic Energy Agency (SPring-8), Hyogo 679-5148, Japan

† Electronic supplementary information (ESI) available. See DOI: 10.1039/c6ra12256f

materials such as boron doped diamond electrodes, carbon/ceramic based composites, nickel based metal complexes, Ag, Au and Pt nanoparticles, organic redox mediators, polymers, polymer composites, RNA modified electrodes and screen printed electrodes.[8] Transition metal oxide nanostructures are a subject of scientific interest owing to their uniqueness and applications (antimicrobial activity, batteries, biomedicine, sensing and solar cells). Nanomaterials with size-specific character have been attained on the nanoscale that are extensively explored for applications in aerospace, catalysis, construction, cosmetics, food packaging, electronics, instruments, magnets, medicines, magnetic devices, optoelectronic devices and sensors. Transition metal nanomaterials (Ag, Au, Cu, Pd and Pt) have been studied for their wide range of catalytic activity under mild conditions.[9]

L-Glutamic acid (2-aminopentanedioic acid, L-GA) is a significant excitatory amino acid neurotransmitter in the mammalian nervous system. Changes in the quantity of L-GA in a particular area of the brain are closely related to Alzheimer's disease and Parkinson's disease.[10] Earlier research has reported that the L-GA rich chains of bone sialoprotein, osteonectin and osteopontin are concerned with Hap nucleation and growth.[11] L-GA is a rich amino acid constituent of plant biomass and is highly attractive for producing industrially significant bio-based chemicals such as 3-cyanopropionate, succinonitrile and γ-aminobutyric acid.[12] It is a well known flavour enhancer and is generally found in different foods. An extreme intake of this flavour enhancer may cause allergic effects (headache and stomach pain).[13] L-GA is a characteristic synthetic amino acid that could be an excellent biopolymer for use in electrochemical sensors owing to its appropriate structure and being green in nature.[14] Uric acid (2,6,8-trihydroxypurine, UA) exists in extracellular fluids of the central nervous system, serum and urine in mammals, is easy to accumulate due to its poor solubility and plays an important role in the function of human metabolism. UA is the preliminary product of adenosine, guanosine and purine metabolism and unusual concentrations result in arthritis, diabetes, gout, high blood pressure, hyperuricemia, hypertension, Lesch–Nyhan syndrome, leukemia, chronic kidney disease, kidney stones, metabolic syndrome, neurological diseases, obesity, pneumonia and renal problems, while low levels in serum can result in cardiovascular disease, multiple sclerosis, Parkinson's, schizophrenia and scurvy. In addition, UA acts as an antioxidant in body fluids and shows counteraction of oxidative damage that occurs in degenerative diseases. Different analytical approaches such as chemiluminescence, colorimetry, electrochemistry, electrophoresis, fluorimetry, HPLC, iodometric titration, spectrophotometry and UV/Vis spectroscopy have been applied for the determination of UA. These methods are complicated and expensive; their limits of detection never meet clinical demands and they are time consuming. Among these techniques, capillary electrophoresis, chemiluminescence, colorimetric, cyclic voltammetry, potentiometric non-enzymatic methods and spectrophotometry can only be used for individual analyte detection. But identification of numerous analytes using these traditional procedures requires multi-channels and bulky potentiostatic circuitry that

restricts their applicability for the simultaneous determination of these biomolecules. Since L-GA and UA are easily oxidizable and electroactive, electrochemical processes have been widely used for their detection.[15–20] Therefore, it is urgently required to introduce an efficient analytical technique for biological stuff. The aim of the present study is to design a novel approach to apply mesoporous Co_3O_4 NSs in the enzyme free simultaneous determination of L-GA and UA by using an $I–V$ method. To best of our knowledge this is the first report of the non-enzymatic simultaneous detection of L-GA and UA using an $I–V$ technique with mesoporous Co_3O_4 NSs.

## 2 Experimental section

2.1. Materials and methods

Chemical reagents of analytical grade such as ethanol, Nafion® (5% ethanolic solution), sodium hydroxide, bilirubin, D-glucose, glycine, L-aspartic acid, L-cystine, L-glutamic acid, L-glutathione, L-tyrosine, thiourea and uric acid were purchased from Sigma Aldrich and used as received. FTIR and UV/Vis spectra of the Co_3O_4 NSs (black powder) were recorded on a Thermo scientific Nicolet iS50 FTIR spectrometer (Madison, WI, USA), and 300 UV-Visible spectrophotometer (Thermo Scientific), respectively. XPS experiments were performed to determine the binding energy between Co and O on a K-α1 spectrometer (Thermo Scientific, K-α1 1066) with an excitation radiation source (A1Kα1, beam spot size = 300.0 μm, pass energy = 200.0 eV, pressure $\sim 10^{-8}$ Torr). N_2 adsorption–desorption isotherms were carried out using a 3Flex analyzer (Micromeritics, USA) at 77 K. Specific surface area (SBET) was calculated using multi-point adsorption data from the linear segment of the N_2 adsorption isotherms using BET theory. Electrochemical properties such as arrangement including elemental analysis, morphology, and particle size of the Co_3O_4 NSs was examined using a FESEM (JEOL, JSM-7600F, Japan) coupled with XEDS. XRD experiments were also conducted under ambient conditions to measure the crystalline pattern of the Co_3O_4 NSs. In order to detect L-GA and UA, $I–V$ technique was performed at a selective point using the fabricated Co_3O_4 NSs by a Keithley electrometer (6517A, USA).

2.2. Preparation of Co_3O_4 nanosheets

Cobalt nitrate $[Co(NO_3)_2 \cdot 6H_2O]$ and sodium hydroxide (NaOH) were used as reacting agents in the preparation of Co_3O_4 NSs using a simple wet chemical method (Scheme 1). The wet chemical method is a classical solid state technique, widely used in the synthesis of doped or undoped nanomaterials, and the product is achieved smaller grains as well as a shorter duration of phase formation. Based on this technique, $Co(NO_3)_2 \cdot 6H_2O$ (0.1 M, 2.92 g) was dissolved in distilled water (100.0 mL) in a conical flask (250.0 mL) under continuous stirring. The pH of the resultant solution was adjusted to 10.19 by adding NaOH, and the solution was then placed at 90.0 °C with continual stirring. After 6 h of continuous stirring, the flask was washed thoroughly with water and acetone consecutively, and then kept for drying in open air (12 h) at room

temperature. The resultant black slurry of Co_3O_4 NSs were dried in an oven at 60.0 °C (24 h), ground into a powder and dried again at 60.0 °C in the oven (24 h) in order to use it for electrochemical measurements. A feasible mechanism for the reactions leading to the formation of Co_3O_4 NSs is as follows [reaction (i)–(vii)].[21]

$$NaOH_{(s)} \rightarrow Na^+_{(aq.)} + OH^-_{(aq.)} \qquad (i)$$

$$Co(NO_3)_2 \rightarrow Co^{2+}_{(aq.)} + 2NO_3^-_{(aq.)} \qquad (ii)$$

$$Na^+_{(aq.)} + 2OH^-_{(aq.)} + Co^{2+}_{(aq.)} + NO_3^-_{(aq.)} \rightarrow Co(OH)^+_{(aq.)}\downarrow + NaNO_{3(aq.)} \qquad (iii)$$

$$Co(OH)^+_{(aq.)} + OH^- \rightarrow Co(OH)_{2(aq.)} \qquad (iv)$$

$$4Co(OH)_2^- + O_2 \rightarrow 4CoOOH + 2H_2O \qquad (v)$$

$$2CoOOH + Co(OH)_2 \rightarrow Co_3O_{4(s)}\downarrow + 2H_2O \qquad (vi)$$

$$3CoOOH + H^+ + e^- \rightarrow Co_3O_{4(s)}\downarrow + 2H_2O \qquad (vii)$$
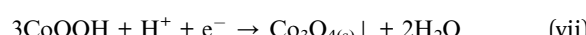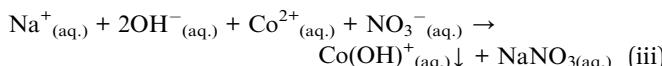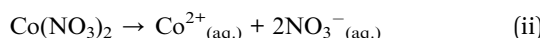
According to the principle of the Ostwald ripening method, Co_3O_4 nucleus growth took place initially by self and mutual aggregation, then the nanocrystals re-aggregated and aggregated Co_3O_4 nanocrystals were formed. The nanocrystals crystallized and re-aggregated with each other's counter parts through van der Waals forces and a spherical Co_3O_4 morphology was reformed (Scheme 2). The doped NSs were characterized in detail in terms of their electrochemical properties (elemental, morphological, optical and structural) and applied in L-GA and UA detection.

2.3. Fabrication of GCE with mesoporous Co_3O_4 NSs

Phosphate buffer saline, PBS (200.0 mL, 0.1 M, pH = 7) was prepared from NaH_2PO_4 (0.2 M), Na_2HPO_4 (0.2 M) and distilled water (200.0 mL). A conducting binder, 5% ethanolic nafion solution was used to fabricate a GCE with Co_3O_4 NSs. The fabricated electrode was then kept at room temperature (6 h) for complete drying with uniform film formation. The fabricated GCE and a platinum (Pt) wire were used as a working and counter electrode, respectively, for the purpose of detecting current–voltage response using I–V technique. Real samples were collected from a local medical center. Initially, the serum
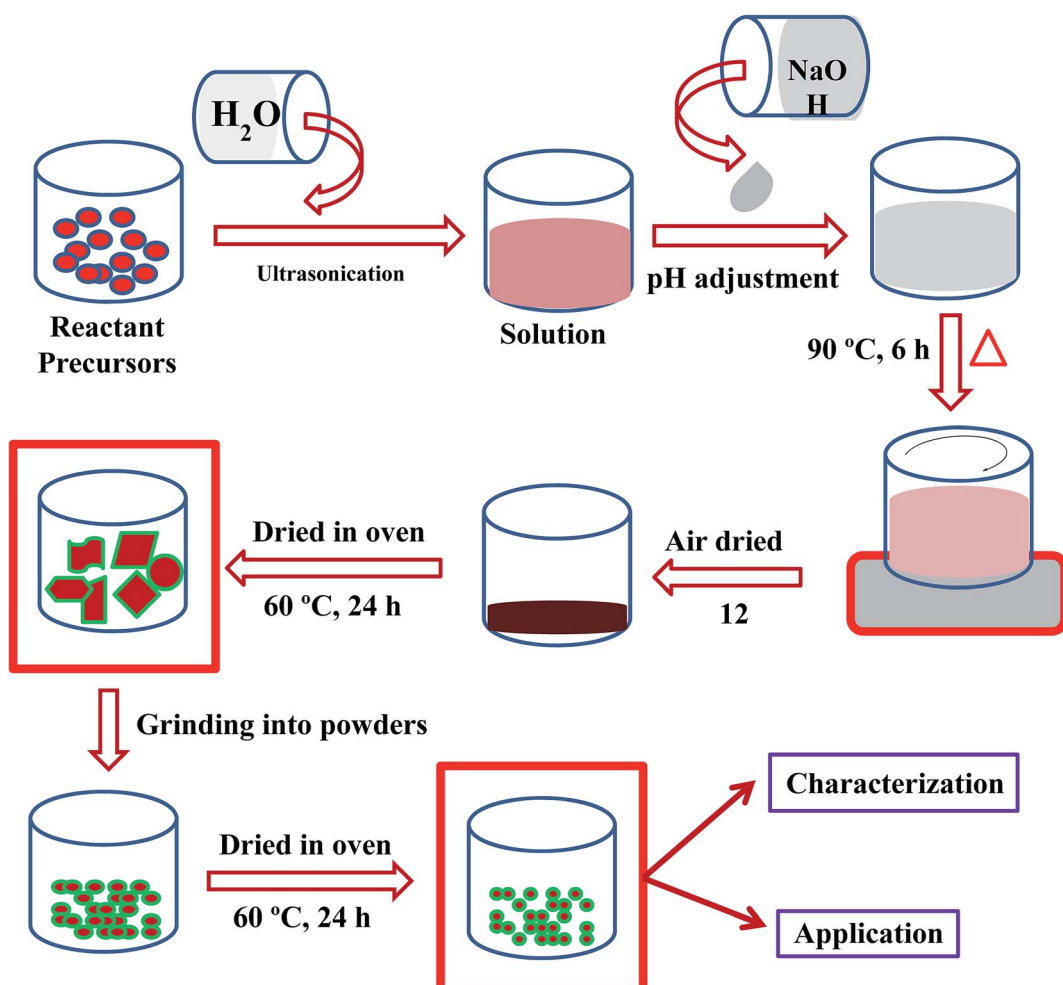
Scheme 1 Schematic diagram of a wet chemical process.
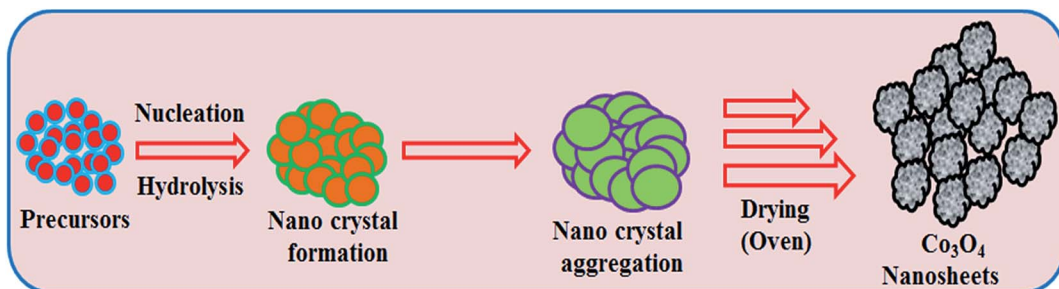
Scheme 2 Growth mechanism of mesoporous Co_3O_4 nanosheets.

was isolated from the blood. After dilution in PBS buffer, serum samples were analyzed with the fabricated Co_3O_4 NSs/GCE sensor by $I-V$ method at room conditions.

3 Results and discussion

3.1. Optical and structural characteristics

Optical features were one of the characteristics considered in the assessment of the photocatalytic activity of the black powder Co_3O_4 NSs. According to UV/visible spectroscopy principles, the spectrum and band gap energy of the metal oxide are attained

due to the adsorption of radiant energy during the shifting of the outer electrons of the atom to an upper energy level. The UV/vis spectrum of the Co_3O_4 NSs was recorded in the visible range (400–800 nm) and a broad absorption band at around 315.7.0 nm was found (Fig. 1a). Upon maximum level band absorption, the band gap energy of the Co_3O_4 NSs was calculated according to Tauc's rule (direct band gap rule, (viii)).[22] $(\alpha h\nu)^2$ $vs.$ $h\nu$ was plotted and then extrapolated to the x-axis, and from the extrapolated curve, the band gap energy for Co_3O_4 NSs was found to be $\sim$2.4 eV (Fig. 1b). Here, α = absorption coefficient, h = Planck's constant, ν = frequency, r = 0.5 (direct transition),
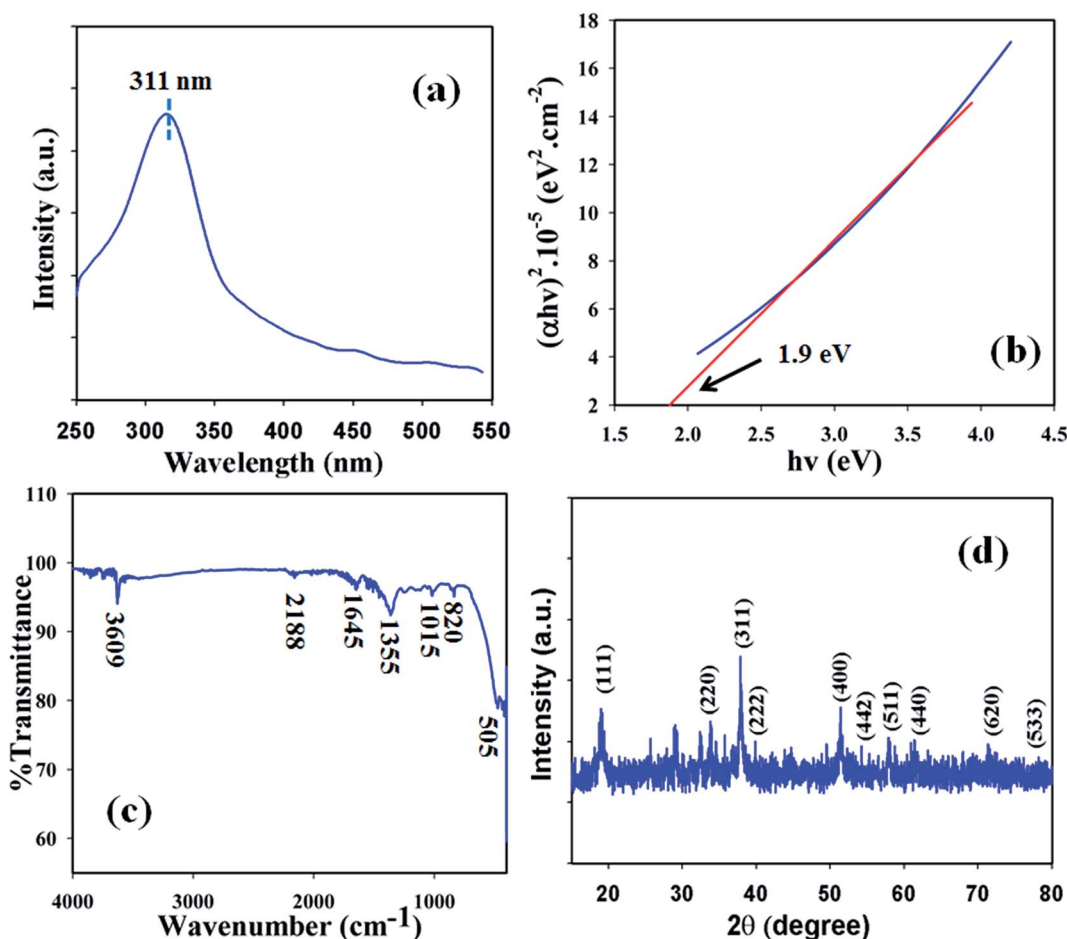
Fig. 1 (a) UV spectrum, (b) band-gap energy plot, (c) FTIR and (d) XRD pattern of the NSs.

A = constant related to the effective mass of the electrons and E_{bg} = band gap energy.

$$(\alpha h\nu)^{1/r} = A(h\nu - E_{bg}) \qquad \text{(viii)}$$

In order to determine the functional character of the Co_3O_4 NSs, FTIR measurements were conducted (region: 4000–400 cm^{-1}) under normal conditions from the perspective of atomic and molecular vibrations. The IR spectrum displays peaks at 3609, 2188, 1645, 1355, 1015, 820, and 505 cm^{-1} which are assigned the presence of O–H (stretching), –C≡C– (stretching), –C=C– (stretching), C–H (rocking), Co–O–Co (stretching), C–H, and Co=O (stretching) in the NSs, respectively (Fig. 1c). The peak at 505 cm^{-1} is given by metal-oxide (Co=O) bond which shows the configuration of Co_3O_4 NSs.[23]

The crystalline nature is an indication of a metal–oxygen framework and at this point, XRD analysis is carried out (2θ = 10–80°) in order to determine the crystalline pattern of the prepared mesoporous Co_3O_4 NSs. Potential peak intensities with a signal for 2θ values are found at 111, 220, 311, 400, 442, 511 and 440 degrees (Fig. 1d) and all the observed peaks in the spectrum are assigned according to the JCPDS file 76-1802. The potential peaks indicate the crystalline pattern and purity of the NSs. Based on the XRD analysis it can be suggested that a good extent of crystalline Co_3O_4 was existed in the prepared NSs.[24]

3.2. Morphological and elemental examination

FESEM is a distinguished method, used to study the morphology of the Co_3O_4 NSs. The morphology including the elemental nature of the prepared black Co_3O_4 NSs was evaluated using FESEM fitted with XEDS. The typical shapes of the black Co_3O_4 NSs were recorded at a low to high magnified range (Fig. 2a and b).[25] On the basis of the XEDS analysis, cobalt (Co) and oxygen (O) are existed in the black mesoporous Co_3O_4 NSs. The NSs contain O (38.12) and Co (61.88) wt% (Fig. 2c and d). No supplementary peaks were observed regarding impurities in the FESEM and XEDS spectra, which indicates that the NSs were composed of O and Co.[24,26]

3.3. Binding energy

XPS is a quantitative spectroscopic technique that was used to determine the chemical nature of the elements present in the Co_3O_4 NSs. The kinetic energy including electron number of a sample can be estimated during XPS examination by irradiation of the nanomaterials with an X-ray beam. Usually, the elemental composition, empirical formula, the chemical, and electronic states of the elements present in a nanomaterial may be investigated using this procedure. According to the XPS analysis, cobalt and oxygen are presented in the prepared Co_3O_4 NSs (Fig. 3a). The O 1s and spin orbit Co $2p_{3/2}$ and Co $2p_{1/2}$ spectra show major peaks at 530.3, 781.0, and 797.0 eV, respectively, which acknowledges that oxygen (O^{2-}) and cobalt

Element	Weight%	Atomic%
O K	57.14	60.08
Co K	42.86	39.92
Totals	100.00	
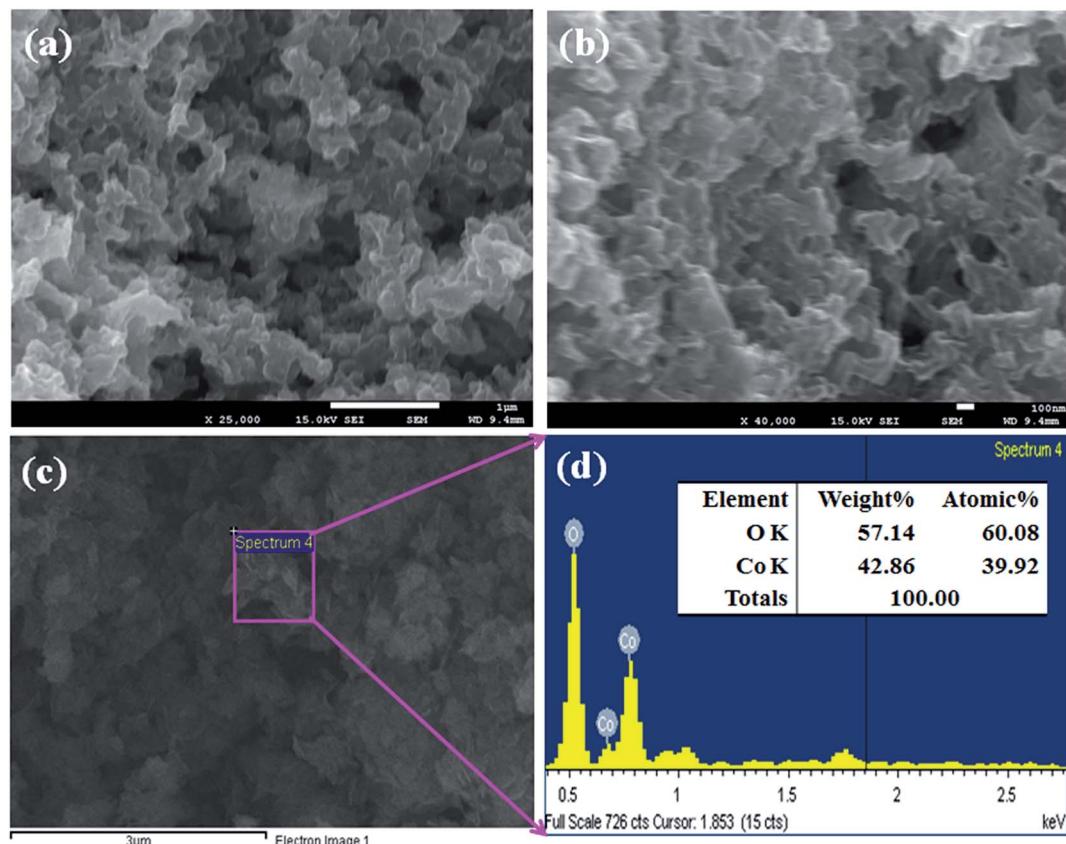
Fig. 2 (a and b) Low and high magnified images and (c and d) elemental analysis of the Co_3O_4 NSs.

(Co^{2+}) are present in the NSs (Fig. 3b and c).[21] The deconvoluted of Co $2p_{1/2}$ peaks were assigned to Co^0, Co^{2+}, and Co^{3+} from low to high binding energy. The binding energy of Co^{3+} with tetrahedral geometry (high spin) was assigned to be lower than that of Co^{2+} with an octahedral structure (low spin).[23]

3.4. BET analysis

Surface characterization of the Co_3O_4 NSs based on the N_2 adsorption–desorption isotherms shows an IV-type isotherm with a hysteresis loop, which is representative of mesoporous ordered framework textural pores judging from the top of Fig. 4. In addition, the mesoporous cobalt oxide nanosheets exhibit a significantly high surface area (S_{BET}), pore volume and pore diameter according to the data analysis (Fig. 4). Also, the N_2 isotherm indicates uniform channels with well pore size with a surface area of 17.93 $m^2 g^{-1}$, high pore volume of 0.11 $cm^3 g^{-1}$ and pore diameter of 35.35 nm. The high surface area of the mesoporous cobalt oxide nanosheets exhibits the case cavities, during the reduction of reactant precursors using alkaline medium in a wet chemical process.
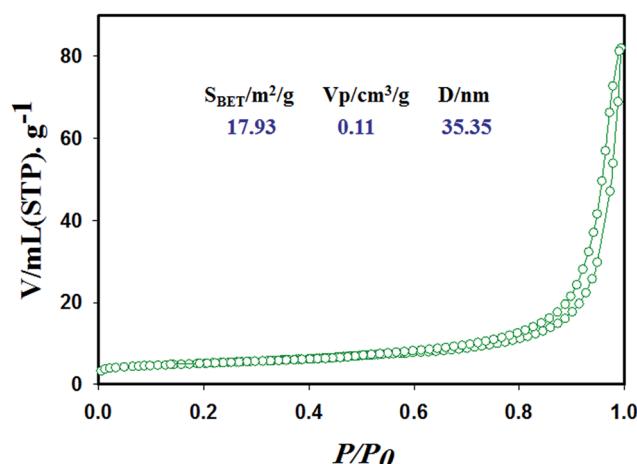
Fig. 4 Surface characterization of the cobalt oxide nanosheets material with specific surface area, pore volume and pore size by N_2 adsorption–desorption isotherms.
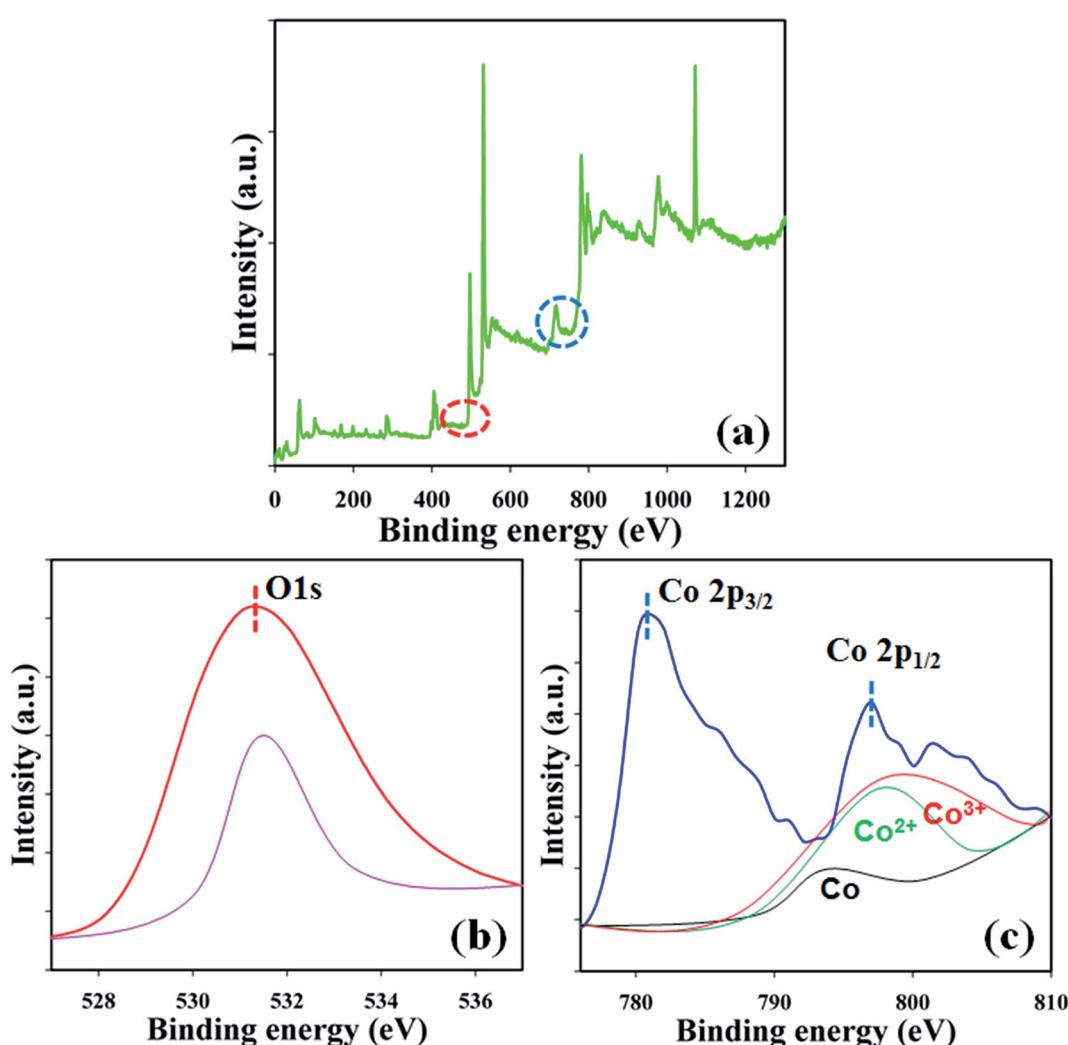
Fig. 3 Binding energy analysis (a) full spectrum, (b) O 1s, and (c) spin orbit Co 2p level of the NSs.

3.5. Application

3.5.1. Detection of ʟ-glutamic acid and uric acid by mesoporous cobalt oxide nanosheets. Expansion of the fabricated electrode with NSs is the preliminary phase of its utilization as a biosensor. The major purpose of the Co_3O_4 NSs assembled as a biosensor onto the GCE was for the identification and quantification of the target analytes, ʟ-GA and UA, in a PBS system. In Scheme 3, the overall fabrication and possible mechanism for the detection of ʟ-GA and UA with Co_3O_4 NSs using an *I–V* technique are presented, where upon oxidation, ʟ-GA and UA are converted into (*E*)-pent-2-enedioic acid and 1*H*-purine-2,6,8(3*H*)-trione, respectively.[27] Both ʟ-GA and UA release two electrons into the sensor system to enhance the *I–V* current significantly *via* intermediate or direct chemical conversion towards (*E*)-pent-2-enedioic acid and 1*H*-purine-2,6,8(3*H*)-trione, respectively.

The Co_3O_4 NSs/GCE sensors possess several advantages such as being chemically inert, easily fabricated, non-toxic, safe and stable in air. The Co_3O_4 NSs assembled onto an electrode as a biosensor has been used to classify blotting agents that are not significantly helpful in a healthcare setting. The pH of the different PBS (pH = 5.7, 6.5, 7, 7.5 and 8) were optimized to distinguish a system which was more suitable to measure ʟ-GA and UA, where pH = 7.5 was found to be more responsive (Fig. 5a) in *I–V* measurements using the Keithley electrometer. The current responses (potential range: 0.1–1.3 V) of the bare GCE, coated Co_3O_4 particles and coated Co_3O_4 NSs electrode are presented in Fig. 5b. The variation of the current response between bare and coated particles/GCE and nanosheets/GCE was examined, where the current signals were enhanced by coating in comparison with the bare GCE and simple cobalt oxide particles. Biological agents such as bilirubin, ᴅ-glucose, glycine, ʟ-aspartic acid, ʟ-cystine, ʟ-glutamic acid, ʟ-glutathione, ʟ-tyrocine, thiourea and uric acid were examined in order to detect the maximum current response to the Co_3O_4 NSs fabricated electrode. Therefore, it was markedly observed that the sensor was more selective towards ʟ-GA and UA compared with other chemicals (Fig. 5c). The current signals without analyte (black dotted) and with analyte (red and blue dotted) were also evaluated under similar conditions by electrochemical performance. An enrichment of current response was observed for the modified Co_3O_4 NSs electrode with ʟ-GA and UA that maintains a large surface region with better coverage in absorption and adsorption potentiality onto the porous NSs exterior of the characteristic element (Fig. 5d).

The shifting of current of the fabricated electrode is a function of ʟ-GA and UA concentration under standard conditions. *I–V* responses of the ʟ-GA and UA with different concentrations towards the Co_3O_4 NSs modified electrode were measured. The current responses were enhanced on the ordinary basis from a lower to higher concentration of the target analytes (Fig. 6a and c). A series of analyte concentrations (0.1 nM to 0.1 M) were examined from a lower to higher potential (0–1.3 V) in order to find out the probable analytical limit. Linear calibration curves at 0.7 V were plotted from the different concentrations of ʟ-GA and UA in a PBS system from a low to high marked
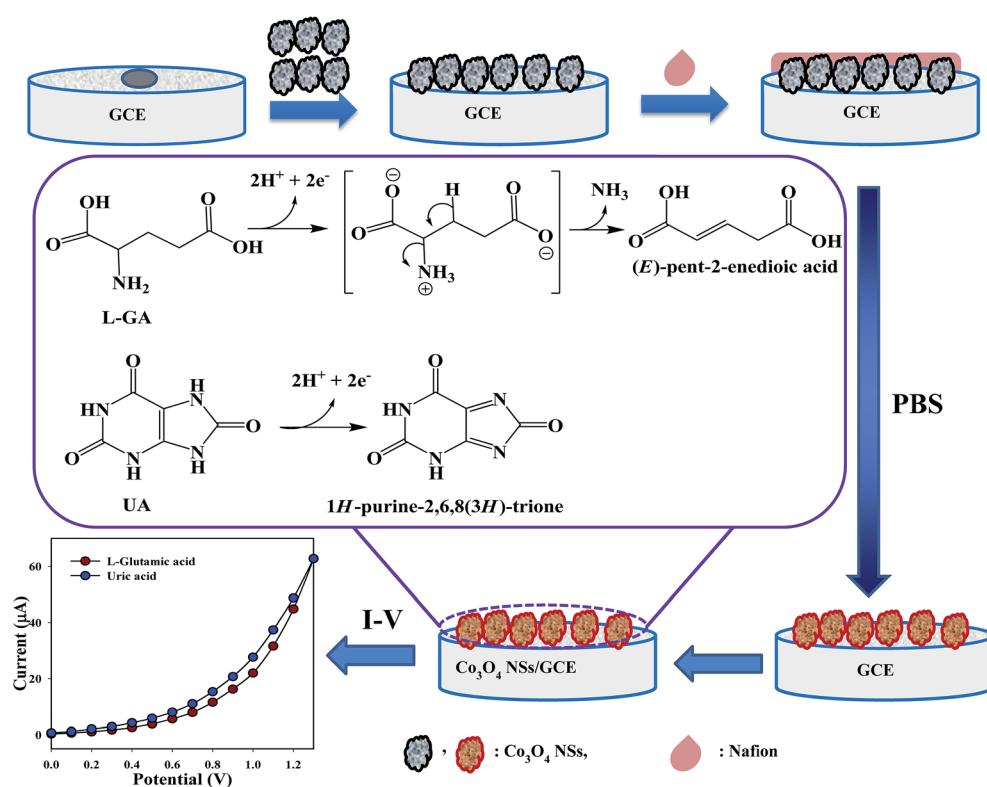
Scheme 3 Fabrication and proposed mechanism for the detection of ʟ-GA and UA by the Co_3O_4 NSs.
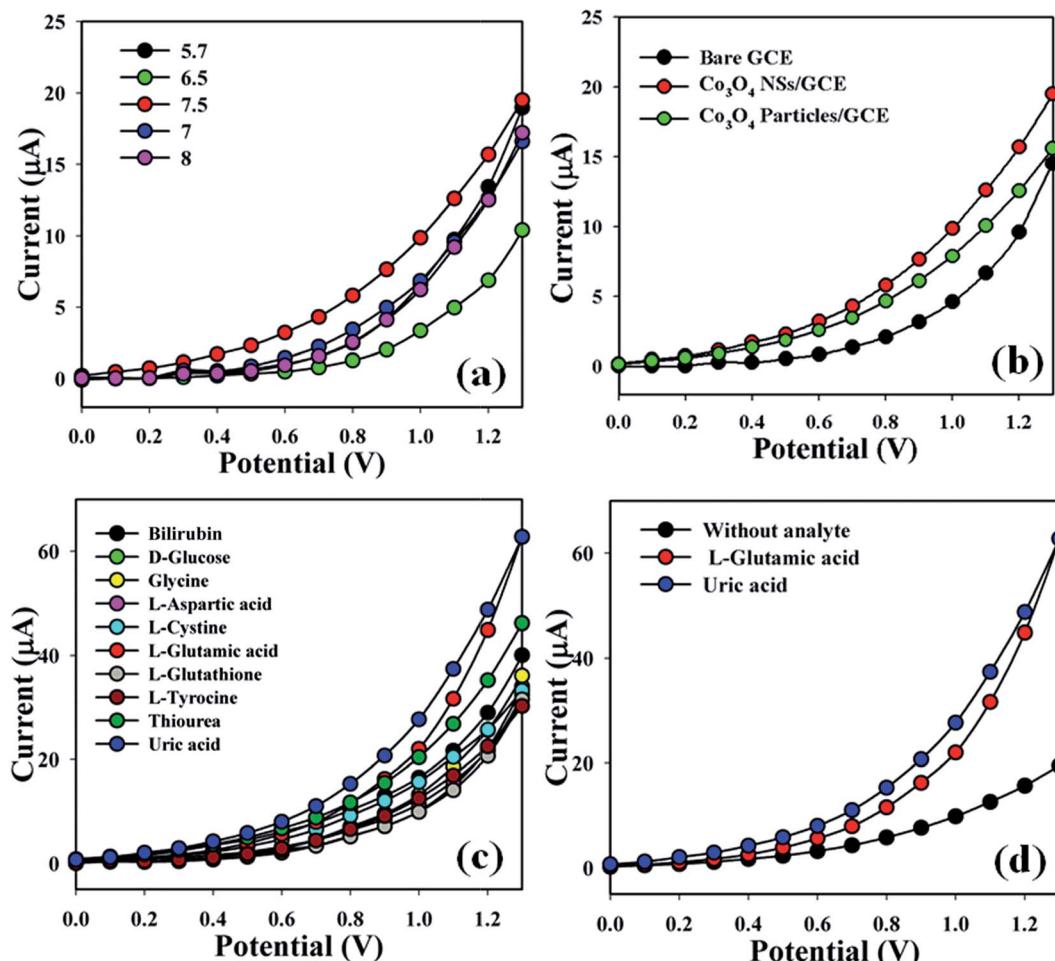
Fig. 5   (a) pH optimization, (b) control experiment (bare, particles, and nanosheet-coated electrodes), (c) selectivity study, and (d) in the absence and presence of analytes.

concentration. The regression coefficient (R^2 = 0.889 and 0.901), sensitivity (9.5×10^{-5} and 1.6×10^{-4} μA μM^{-1} cm^{-2}) and limit of detection (10.0 and 60 pM) of L-GA and UA, respectively, were calculated from the calibration curve at a signal-to-noise ratio = 3 (Fig. 6b and d). LDR (1.0 nM to 0.1 M) and response time of the electrode were also acquired from the realistic concentration deviation graph.

The sensing capability of the Co_3O_4 NSs coated electrode was measured for up to two weeks in order to find out its reproducibility and storage ability. A sequence of nine and ten successive measurements of L-GA and UA solutions (1.0 μM) was examined, and excellent reproducible responses were found with the Co_3O_4 NSs electrode under the identical conditions. It is recognized that the I–V responses do not extensively change after washing of the fabricated Co_3O_4 NSs electrode in each experiment (Fig. 7a and b). Almost similar sensitivity was retained as the initial response for up to two weeks; after that the response of the fabricated electrode decreases regularly. The response of the NSs sensor was considered with respect to the storage time to determine its long term storage ability. The storage ability of the Co_3O_4 NSs electrode sensor was evaluated under normal conditions and the sensitivity was maintained

almost 90% relative to the regular response for a number of days. It is clear that the fabricated sensor can be used without any significant loss of sensitivity for up to many days. An assessment of L-GA and UA identification using different techniques is presented in Table 1.

3.5.2.   Real sample analysis. In order to validate the legitimacy of the I–V technique, the Co_3O_4 NSs were used to determine L-GA and UA concentrations in different real samples (serum and urine). The standard addition method used in the original sample study was used to measure the concentration of L-GA and UA. A fixed amount (~25.0 μL) of each bulk solution was mixed and analyzed in PBS (10.0 mL, 0.1 M) using the fabricated Co_3O_4 NSs electrodes. The results show that the detection of L-GA and UA in serum and urine samples is possible, which actually establishes that the I–V scheme is suitable for analyzing real samples with the Co_3O_4 NSs materials (Table 2).

4   Conclusion

Co_3O_4 NSs were synthesized using a simple wet chemical technique in an alkaline medium. The optical properties of the
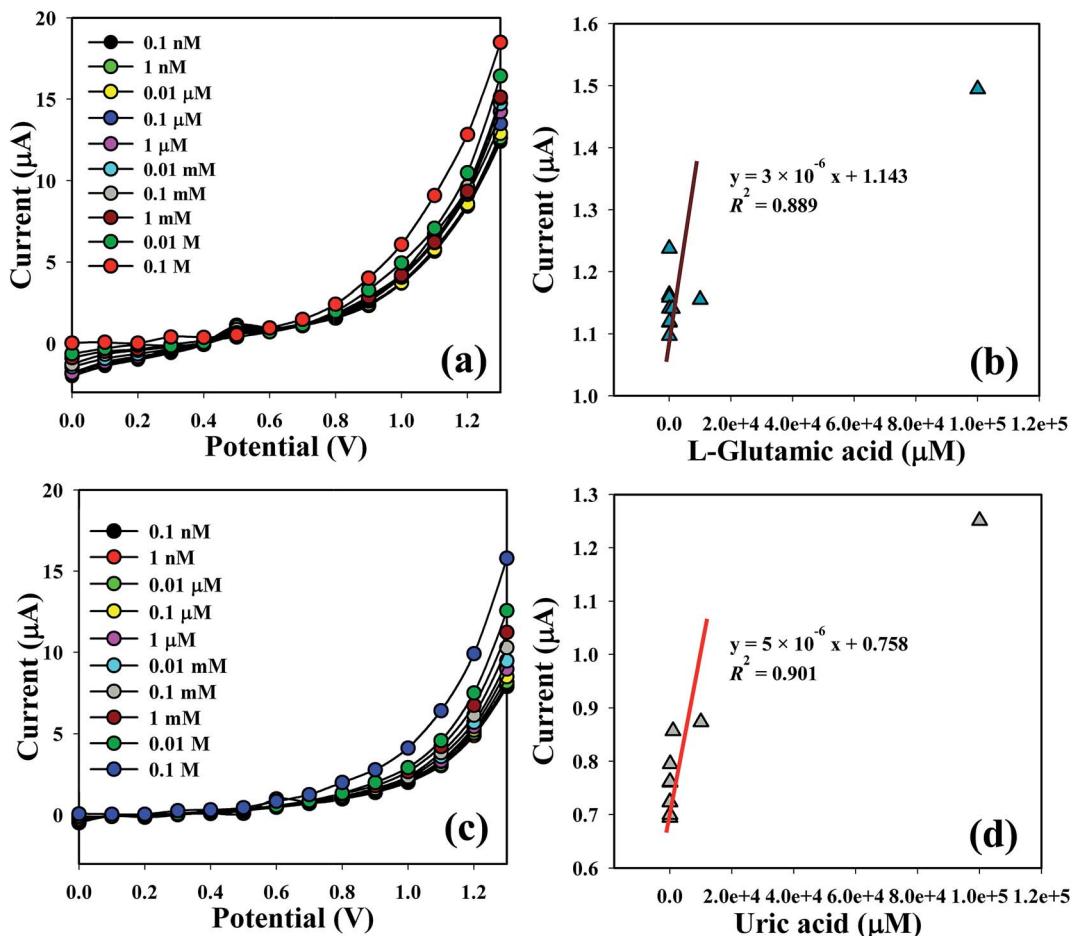
Fig. 6 Co_3O_4 NSs coated GCE for sensing by $I-V$ response with (a and c) concentration variation; (b and d) are the calibration curves of L-GA and UA, respectively.

NSs were examined using electrochemical techniques such as UV/vis, FT-IR, FESEM, XEDS, XPS and XRD. A simple fabrication process was applied in order to modify a GCE with Co_3O_4 NSs using a conducting binder. Selective and sensitive L-GA and UA

biosensors were fabricated successfully based on the GCE assembled with Co_3O_4 NSs using an $I-V$ method. The electrochemical performance of the fabricated L-GA and UA biosensors was excellent in terms of detection limit, linear dynamic range,
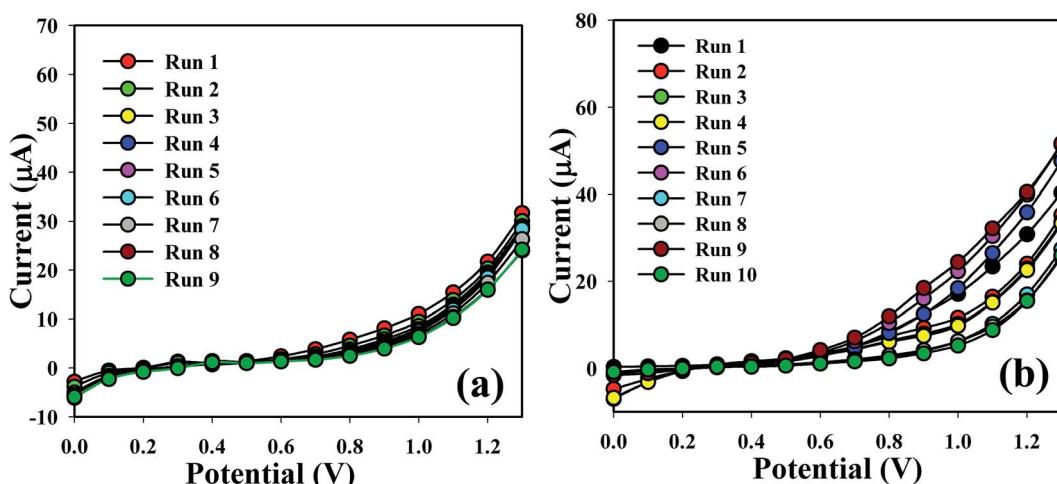
Fig. 7 Repeatability study of (a) L-GA and (b) UA.

Table 1 Detection of L-GA and UA using different analytical methods[a]

Analytes	Methods	Sensitivity ($\mu A\ \mu M^{-1}\ cm^{-2}$)	LDR (μM)	LOD (μM)	Ref.
L-GA	HPLC	—	1.0×10^{-8} to 1.0×10^{-6} M	1.0×10^{-9} M	10
	RM + CM	—	—	7.96×10^{-7} M	28
	I–V	**9.5×10^{-5}**	**0.1 nM to 0.1 M**	**10 pM**	**This work**
UA	HPLC-UV	—	1.7–4.0	1.42	29
	Enzymatic-fluorescence	—	0.2–6.0	0.10	30
	Dual enzyme-fluorescence	—	125.0–1000.0	125	31
	Enzymetric-UV absorption	—	2.0–200.0	0.36	32
	Potentiometric non-enzymatic	—	—	0.50	33
	Fluorometric	—	0.4–3.6	0.10	34
	Flow-injection chemiluminescence	—	0.4–200.0	0.12	35
	Capillary electrophoresis	—	0.6–30.0	0.35	36
	Electrochemical	—	0.2–500.0	0.16	37
	I–V	**1.6×10^{-4}**	**0.1 nM to 0.1 M**	**60 pM**	**This work**

[a] HPLC = high performance liquid chromatography, RM = ratiometric, CM = colorimetric.

Table 2 Measured concentration of the analytes in real samples[a]

Real samples	Observed current (μA)				Calculated conc. (μM)	SD
	R1	R2	R3	Average		
Serum	14.9	8.1	6.7	9.9	13.7	4.4
Urine	16.3	9.7	7.6	11.2	15.5	4.5

[a] R = reading, SD = standard deviation.

sensitivity, repeatability, and short response time. The Co$_3$O$_4$ NSs/GCE electrode is exhibited higher sensitivity (9.5×10^{-5} and 1.6×10^{-4} $\mu A\ \mu M^{-1}\ cm^{-2}$) and a lower detection limit (10.0 and 60.0 pM) for L-GA and UA, respectively, compared to the already published in literature. A competent technique can be introduced by this novel progress in biosensor development in a wide range of biomedical fields.

Acknowledgements

References

1 H. Hou, Y. Fan, S. Wang, L. Si and B. Li, *J. Funct. Foods*, 2016, **24**, 37–47.

2 F. R. R. Teles, D. M. F. Prazeres and J. L. L. Filho, *Sensors*, 2007, **7**, 2510–2518.

3 S. Kim, J. I. Kim, H. R. Park, M. K. Kim, Y. Chong and W. S. Yeo, *Bull. Korean Chem. Soc.*, 2009, **30**, 2574–2576.

4 K. F. Lee, H. M. Cheng, H. C. Hsu, L. J. Lin and W. F. Hsieh, *Phys. Lett.*, 2005, **409**, 208.

5 M. M. Rahman, *PLoS One*, 2014, **9**, e100327.

6 A. Ohtomo, M. Kawasaki, Y. Sakurai, I. Ohkubo, R. Shiroki, Y. Yoshida, T. Yasuda, Y. Segawa and H. Koinuma, *Mater. Sci. Eng., B*, 1998, **56**, 263.

7 S. Mallakpour, M. Dinari and S. Neamani, *Prog. Org. Coat.*, 2015, **86**, 11–17.

8 A. Joshi, W. Schuhmann and T. C. Nagaiah, *Sens. Actuators, B*, 2016, **230**, 544–555.

9 S. Shinde, H. Dhaygude, D.-Y. Kim, G. Ghodake, P. Bhagwat, P. Dandge and V. Fulari, *J. Ind. Eng. Chem.*, 2016, **36**, 116.

10 L. Xin, L. Jie, L. C. Wei and Z. S. Lin, *Chin. J. Anal. Chem.*, 2007, **35**, 1151–1154.

11 M. P. Gashti, M. Bourquin, M. Stir and J. Hulliger, *J. Mater. Chem. B*, 2013, **1**, 1501–1508.

12 F. D. Schouwer, L. Claes, N. CLaes, S. Bals, J. Degreve and D. E. D. Vos, *Green Chem.*, 2015, **17**, 2263–2270.

13 A. Ghorai, J. Mondal, R. Chandra and G. K. Patra, *Anal. Methods*, 2015, **7**, 8146–8151.

14 M. P. N. Bui, C. A. Li and G. H. Seong, *BioChip J.*, 2012, **6**, 149–156.

15 H. Hu, Y. Song, M. Feng and H. Zhan, *Electrochim. Acta*, 2016, **190**, 40–48.

16 J. Wnag, Y. Chang, W. B. Wu, P. Zhang, S. Q. Li and C. Z. Huang, *Talanta*, 2016, **152**, 314–320.

17 N. Lavanya, E. Fazio, F. Neri, A. Bonavita, S. G. Leonardi, G. Neri and C. Sekar, *Sens. Actuators, B*, 2015, **221**, 1412–1422.

18 S. S. M. Hassan and N. M. H. Rizk, *Analyst*, 1997, **122**, 815–819.

19 K. Arora, M. Tomar and V. Gupta, *Analyst*, 2014, **139**, 4606–4612.

20 Y. Peng, D. Zhang and C. Zhang, *Anal. Methods*, 2014, **6**, 8965–8972.

21 L. M. Alrehaily, J. M. Joseph, M. C. Biesinger, D. A. Guzonas and J. C. Wren, *Phys. Chem. Chem. Phys.*, 2013, **15**, 1014–1024.

22 M. F. Silva, L. A. S. de-Oliveira, M. A. Ciciliati, L. T. Silva and B. S. Pereira, *J. Appl. Phys.*, 2013, **114**, 104311–104317.

23 A. Altavilla and E. Ciliverto, *Appl. Phys. A*, 2004, **79**, 309.

24 C. Xu, X. Wang, J. Zhu, X. Yang and L. Lu, *J. Mater. Chem.*, 2008, **18**, 5625–5629.

25 S. Harish, K. Silambarasan, G. Kalaiyarasan, A. V. N. Kumar and J. Joseph, *Mater. Lett.*, 2016, **165**, 115–118.

26 X. Lu, X. Huang, S. Xie, T. Zhai, C. Wang, P. Zhang, M. Yu, W. Li, C. Laing and Y. Tong, *J. Mater. Chem.*, 2012, **22**, 13357–13364.

27 Y. Liu, P. She, J. Gong, W. Wu, S. Xu, J. Li, K. Zhao and A. Deng, *Sens. Actuators, B*, 2015, **221**, 1542–1553.

28 A. Ghorai, J. Mondal, R. Chandra and G. K. Patra, *Anal. Methods*, 2015, **7**, 8146–8151.

29 R. Kandar, P. Drabkova and R. Hampl, *J. Chromatogr. B: Anal. Technol. Biomed. Life Sci.*, 2011, **879**, 2834–2839.

30 D. Jin, M. H. Seo, B. T. Huy, Q. T. Pham, M. L. Conte, D. Thangadurai and Y. I. Le, *Biosens. Bioelectron.*, 2016, **77**, 359–365.

31 N. E. Azmi, N. I. Ramli, J. Abdullah, M. A. A. Hamid, H. Sidek, S. A. Rahman, N. Ariffin and N. A. Yousuf, *Biosens. Bioelectron.*, 2015, **67**, 129–133.

32 H. Zhao, Z. Wang, X. Jiao, L. Zhang and Y. Lv, *Spectrosc. Lett.*, 2012, **45**, 511–519.

33 W. Guan, X. Duan and M. A. Reed, *Biosens. Bioelectron.*, 2014, **51**, 225–231.

34 T. Zhang, X. Sun and B. Liu, *Spectrochim. Acta, Part A*, 2011, **79**, 1566–1572.

35 C. Yang and Z. Zhang, *Talanta*, 2010, **81**, 477–481.

36 S. Zhao, J. Wang, F. Ye and Y. M. Liu, *Anal. Biochem.*, 2008, **378**, 127–131.

37 M. Noorozifar, M. K. Motlagh, F. Z. Jahromi and S. Rostami, *Sens. Actuators, B*, 2013, **188**, 65–72.